BUTTERWORTH HEINEMANN

Three-dimensional and heat-loss effects on turbulent flow in a nominally two-dimensional cavity

N. Z. Ince and B. E. Launder
Department of Mechanical Engineering, UMIST, Manchester, UK

This paper reports numerical explorations of turbulent natural convection in a cavity of 5:1 aspect ratio, the heated and cooled surfaces (long sides) being vertical. An extended form of $k-\varepsilon$ eddy viscosity model is adopted, which had earlier been employed to study the same flow assuming two-dimensional (2-D) motion with perfectly insulating end walls. The present computations consider the three-dimensional (3-D) behavior and allow realistic heat losses through the nominally adiabatic surfaces. These generalizations, particularly the latter, account for most of the differences that had hitherto existed between the experiment and computations.

Keywords: turbulent flow; buoyant flow; heat transfer

Introduction

Some years ago, the authors (Ince and Launder, 1989) proposed a variant of the usual $k-\varepsilon$ model and showed that it allowed generally satisfactory prediction of naturally driven two-dimensional (2-D) flow in tall cavities with one heated and one cooled vertical wall (well-insulated horizontal walls being taken as adiabatic). Some features of the predictions remained at odds with the experiments, however. In particular, the significant measured departure from antisymmetry in the measured velocity and temperature profiles could not be closely reproduced, although full account was taken of the temperature dependence of the thermophysical properties of the fluid.

Recently, the opportunity has arisen to re-examine this problem with the substantially greater computational resource now available. This has allowed an exploration of whether the mean flow motions in the third direction could have been responsible. Account has also been taken of probable heat losses from the insulated surfaces. The present contribution reports the outcome of that study.

Mathematical and numerical model

The geometry considered is shown in Figure 1; it is the 5:1 aspect ratio cavity studied by Cheesewright and colleagues. Our earlier study (Ince and Launder 1989) had examined just the hatched plane in the foreground while in the present exploration, half the cavity is considered that extends from the back wall, $A'B'C'D'$, to the hatched plane of symmetry, $ABCD$. The heated and cooled faces ($A'AD'$ and $B'BCC'$) are assigned the uniform temperatures reported in the experiments (Cheesewright et al. 1986; Cheesewright and Lerokipiotis, 1982). On all the other "insulated" walls, the finite thermal resistance between the outside ambient air at 20°C and the

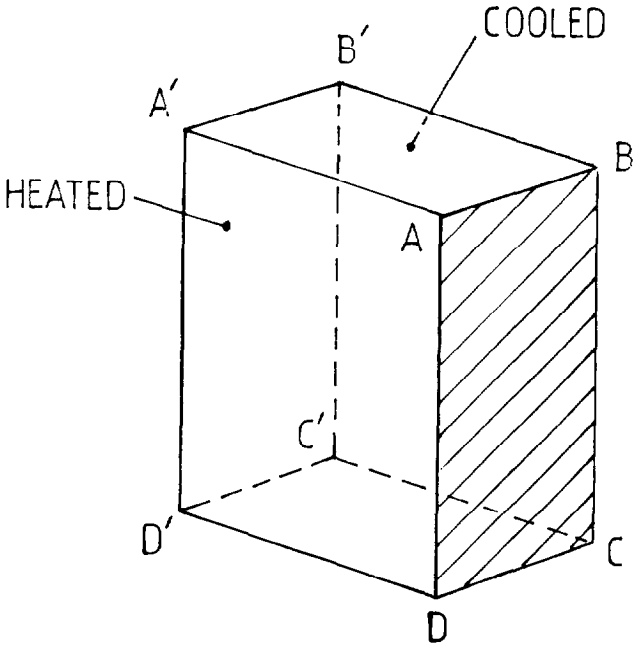

Figure 1 The flow section considered (*ABCD* center) plane; *A'B'C'D'* side wall)

Address reprint requests to Professor B. E. Launder, Department of Mechanical Engineering, UMIST, Manchester M60 1QD, UK.

Received 21 October 1994; accepted 21 February 1995

Int. J. Heat and Fluid Flow 16: 171–177, 1995

655 Avenue of the Americas, New York, NY 10010

0142-727X/95/$10.00
SSDI 0142-727X(95)0015-I

inner surface of the cavity was taken as that associated with conduction through 1 cm of perspex and 5 cm of insulant (with a thermal conductivity of 0.04 W/mK), as indicated in the experiment, plus that attributable to the natural convection on the outside wall. For the latter, different Nusselt–Rayleigh number correlations were taken (Ozisik 1977), depending upon the orientation of the wall. For the vertical surfaces, the following expressions were used:

$$\mathrm{Nu}_L = 0.59\,(\mathrm{Gr}_L\mathrm{Pr})^{1/4} \qquad \mathrm{Gr}_L \le 10^9 \tag{1a}$$

$$\mathrm{Nu}_L = 0.10\,(\mathrm{Gr}_L\mathrm{Pr})^{1/3} \qquad \mathrm{Gr}_L > 10^9 \tag{1b}$$

On the horizontal walls, the following were adopted:

Upward facing surface:

$$\mathrm{Nu}_L = 0.54\,(\mathrm{Gr}_L\mathrm{Pr})^{1/4} \qquad \mathrm{Gr}_L \le 2\times 10^7 \tag{2a}$$

$$\mathrm{Nu}_L = 0.14\,(\mathrm{Gr}_L\mathrm{Pr})^{1/3} \qquad \mathrm{Gr}_L > 2\times 10^7 \tag{2b}$$

Downward facing surface:

$$\mathrm{Nu}_L = 0.27\,(\mathrm{Gr}_L\mathrm{Pr})^{1/4} \tag{3}$$

These may seem rather crude estimates in relation to the detailed numerical treatment applied to the interior of the cavity, but they are, arguably, about the best available. Moreover, they are sufficient to reveal the differences in the interior flow pattern associated with the different physical situations.

The turbulence model employed in the cavity is of the low-Reynolds number $k-\varepsilon$ eddy-viscosity type with the two modifications employed in Ince and Launder (1989); namely, the use of the Yap correction (Launder 1988) to reduce near-wall length scales when turbulence energy generation becomes less than dissipation, and use of the generalized gradient diffusion hypothesis (GGDH) (Daly and Harlow 1970) to represent heat transport. Unlike the usual (simple) gradient transport model, the GGDH can produce substantial heat fluxes at right angles to the mean temperature gradient, and this is quite important in accounting for buoyant effects in the vertically moving boundary layers on the actively heated and cooled surfaces. The complete mathematical statement of the turbulence model is given in Table 1.

Table 1 Turbulence model adopted (from Ince and Launder 1989)

$$-\rho\overline{u_iu_j} = \mu_t\left(\frac{\partial U_i}{\partial x_j}+\frac{\partial U_j}{\partial x_i}\right)-\frac{2}{3}\delta_{ij}\rho k$$

$$-\overline{u_j\theta} = \frac{3}{2}\frac{c_\mu}{\sigma_\theta}\frac{k}{\tilde{\varepsilon}}\overline{u_iu_k}\frac{\partial\Theta}{\partial x_k}$$

where $\mu_t = \rho c_\mu k^2/\tilde{\varepsilon}$ *and* k and $\tilde{\varepsilon}$ are obtained from

$$\rho\frac{Dk}{Dt} = P_k - \varepsilon + \frac{\partial}{\partial x_j}\left[\left(\mu+\frac{\mu_t}{\sigma_\mu}\right)\frac{\partial k}{\partial x_j}\right]$$

$$\rho\frac{D\tilde{\varepsilon}}{Dt} = c_{\varepsilon1}\frac{\tilde{\varepsilon}}{k}P_k - c_{\varepsilon2}\rho\frac{\tilde{\varepsilon}^2}{k} + 2\frac{\mu\mu_t}{\rho}\left(\frac{\partial^2U_i}{\partial x_k\partial x_j}\right)^2 + c_Y\frac{\ell}{\ell_e}\left(1-\frac{\ell}{\ell_e}\right)\frac{\rho\tilde{\varepsilon}^2}{k} + \frac{\partial}{\partial x_j}\left[\left(\mu+\frac{\mu_t}{\sigma_\varepsilon}\right)\frac{\partial\tilde{\varepsilon}}{\partial x_j}\right]$$

where $\ell \equiv k^{3/2}/\tilde{\varepsilon}$; $\ell_e = 2.5x_n$

where x_n is the shortest distance to a wall

$$P_k \equiv -\rho\overline{u_iu_j}\frac{\partial U_i}{\partial x_j} - \beta\rho\overline{u_j\theta}g_i$$

$c_\mu = 0.09\exp -3.4/(1+R_t/50)^2$; $\sigma_\theta = 0.9$; $\sigma_k = 1.0$; $\sigma_\varepsilon = 1.3$; $c_{\varepsilon1} = 1.44$; $c_{\varepsilon2} = 1.92[1-0.3\exp -R_t^2]$; $c_Y = 0.83$; $R_t \equiv \rho k^2/\mu\tilde{\varepsilon}$

Boundary conditions $k = \tilde{\varepsilon} = 0$ at walls

$$\frac{\partial k}{\partial x_n} = \frac{\partial\tilde{\varepsilon}}{\partial x_n} = 0 \qquad \text{at symmetry plane}$$

The numerical computations were performed with a specially adapted version of the TEAM code (Huang and Leschziner 1983). This finite-volume solver employs the velocity components and pressure as dependent variables together with the mean temperature Θ, the turbulence energy k and $\tilde{\varepsilon}$. The

Notation

c_p	specific heat at constant pressure
g	gravitational acceleration
g_i	gravitational acceleration vector, $0, -g, 0$
Gr_L	Grashof number based on side length $\rho^2 g\beta(T_w - T_c)L^3/\mu^2$
k	turbulent kinetic energy
L	side length
Nu_L	Nusselt number on exterior surfaces of cavity based on length of surface
$\overline{\mathrm{Nu}}$	computed vertically averaged value of Nusselt number on inner surface of cavity
$\overline{\mathrm{Nu}}_0$	$\overline{\mathrm{Nu}}$ at $z = 0$ for adiabatic secondary surfaces
P_k	generation rate of turbulent kinetic energy
Pr	molecular Prandtl number
R_t	turbulent Reynolds number, $\rho k^2/\mu\varepsilon$
U_i	mean velocity in direction, x_i
$\overline{u_iu_j}$	kinematic Reynolds stress
$\overline{u_j\theta}$	kinematic turbulent heat flux
x	horizontal coordinate with origin at left (hot) surface
x_i	Cartesian space coordinate
y	vertical coordinate with origin at lower edge of cavity
z	horizontal coordinate parallel to heated and cooled walls with origin at midplane

Greek

β	volumetric expansion coefficient
$\Delta\Theta$	temperature excess above ambient or midplane value
ε	turbulence energy dissipation rate
$\tilde{\varepsilon}$	part of ε associated with spectral transfer, $\tilde{\varepsilon} \equiv \varepsilon - 2\nu(\partial k^{1/2}/\partial x_j)^2$
θ	temperature fluctuation
Θ	local mean temperature (absolute scale)
κ	thermal conductivity
λ	thermal diffusivity, $\kappa/\rho c_p$
μ	dynamic viscosity
μ_t	turbulent viscosity
ν	kinematic viscosity
ρ	density
σ_s	turbulent Prandtl number for ϕ transport ($\phi = \Theta, k, \varepsilon$)

velocity components are staggered relative to the scalar nodes, each being located at the midpoint of the face of the control volume perpendicular to the velocity direction. This "staggering" practice improves stability and has no adverse consequences in the simple rectilinear solution domain considered here. The usual SIMPLE algorithm is employed to iterate between velocity and pressure. Quadratic upwind differencing (the QUICK scheme, Leonard 1979) is employed to achieve accurate handling of convective transport with acceptable stability characteristics. In Ince et al. (1993), we show that, with this differencing strategy and the grid and turbulence model adopted here, numerical errors in Nusselt number and peak velocity are below 2%.

In all cases, iteration to the converged solution was flagged by the usual requirement that overall normalized residuals for all the dependent variables had fallen to a negligible level.

Results and discussion

Two sets of 3-D flow results are considered: the 3-D cavity flow with boundary conditions, as discussed above, and the same geometry but with perfectly adiabatic side, top, and bottom walls. The solution domain extended in the z direction from the vertical center plane to the side wall, in the x direction from the heated to the cooled surface and, in the y direction, from the top to bottom of the cavity. The grids employed were $60 \times 60 \times 30$ for the x, y, and z directions. As noted above, our earlier tests had shown that in a 2-D cavity the 60×60 grid gave sensibly grid-independent results. Comparison is drawn with the experimental data of Cheesewright and his colleagues (Cheesewright et al. 1986; Cheesewright and Lerokipiotis 1982) in which the cavity comprised two vertical facing surfaces measuring 2.5 m × 1.0 m maintained at nominally uniform temperatures of 77.5°C and 31.5°C and enclosed by smooth, insulated walls. The active surfaces were 0.5 m apart horizontally. Two-dimensional computations were also made, effectively, of the section $ABCD$, using a 60×60 mesh.

The very substantial effect of including heat losses in the 3-D calculations is seen in Figure 2, which shows mean temperature profiles on three horizontal planes within the cavity. The

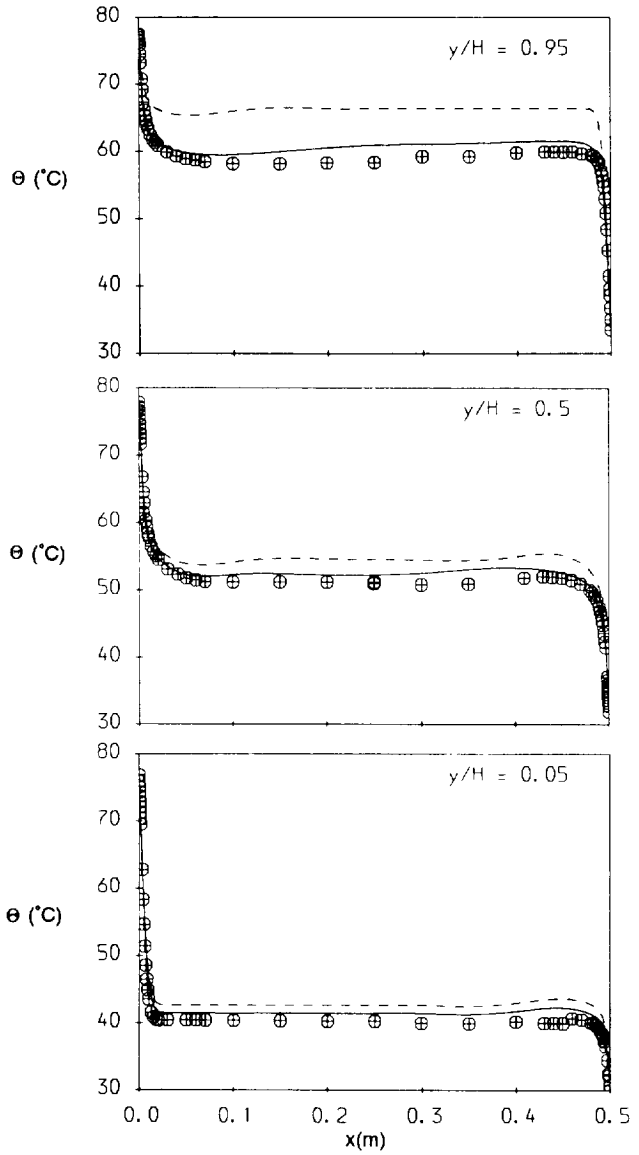

Figure 2 Temperature profiles between heated and cooled walls at $z = 0$; ⊕ experiments; —— computations including heat losses; and - - - - computations with zero heat losses

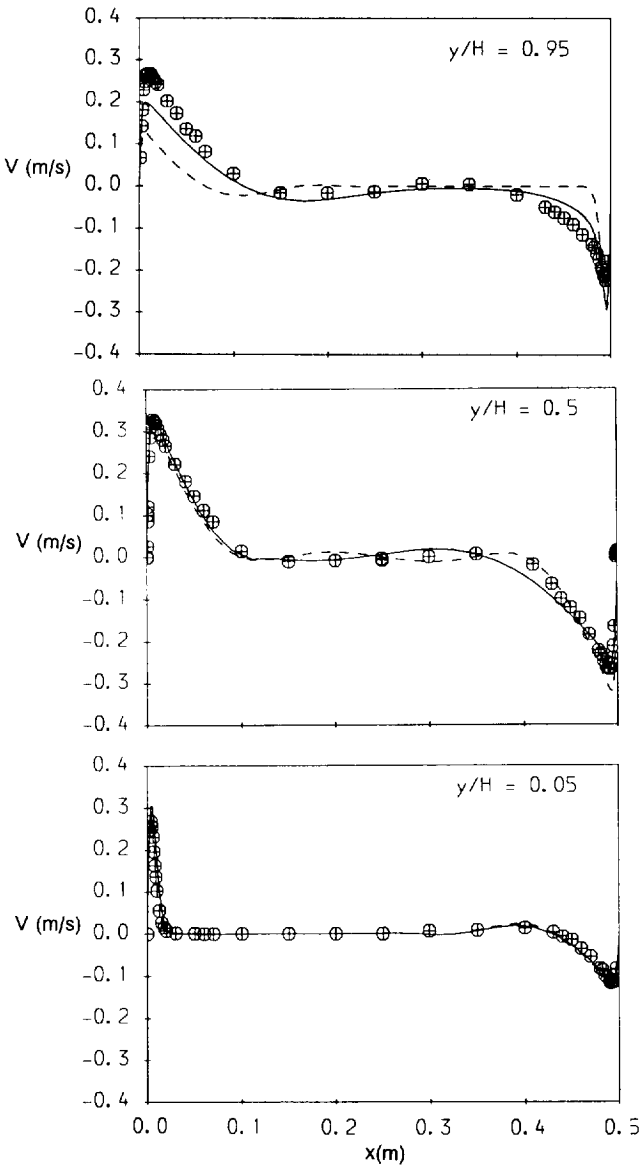

Figure 3 Mean velocity profiles between heated and cooled walls $z = 0$; key as in Figure 2

principal effect is seen near the top of the cavity ($y/H = 0.95$), because it is there that the fluid is hottest, providing a large temperature difference between the inside of the top wall and the external atmosphere. By contrast, there is little heat transfer from the lower surface, because the fluid is cooled to nearly the temperature of the external environment. The effects on the mean velocity profile, Figure 3, are not as strong but, at midheight in the cavity ($y/H = 0.5$), the appreciably different peak velocities in the upward- and downward-moving boundary layer near the heated and cooled vertical wall are captured for the first time. Indeed, it may be remarked that at $y/H = 0.5$, the predictions show a slightly stronger asymmetry than the measurements, although, at $y/H = 0.95$, the very substantial effect is slightly underestimated.

For the case of nonadiabatic walls, Figure 4 shows velocity vectors on the two vertical symmetry planes of the cavity.

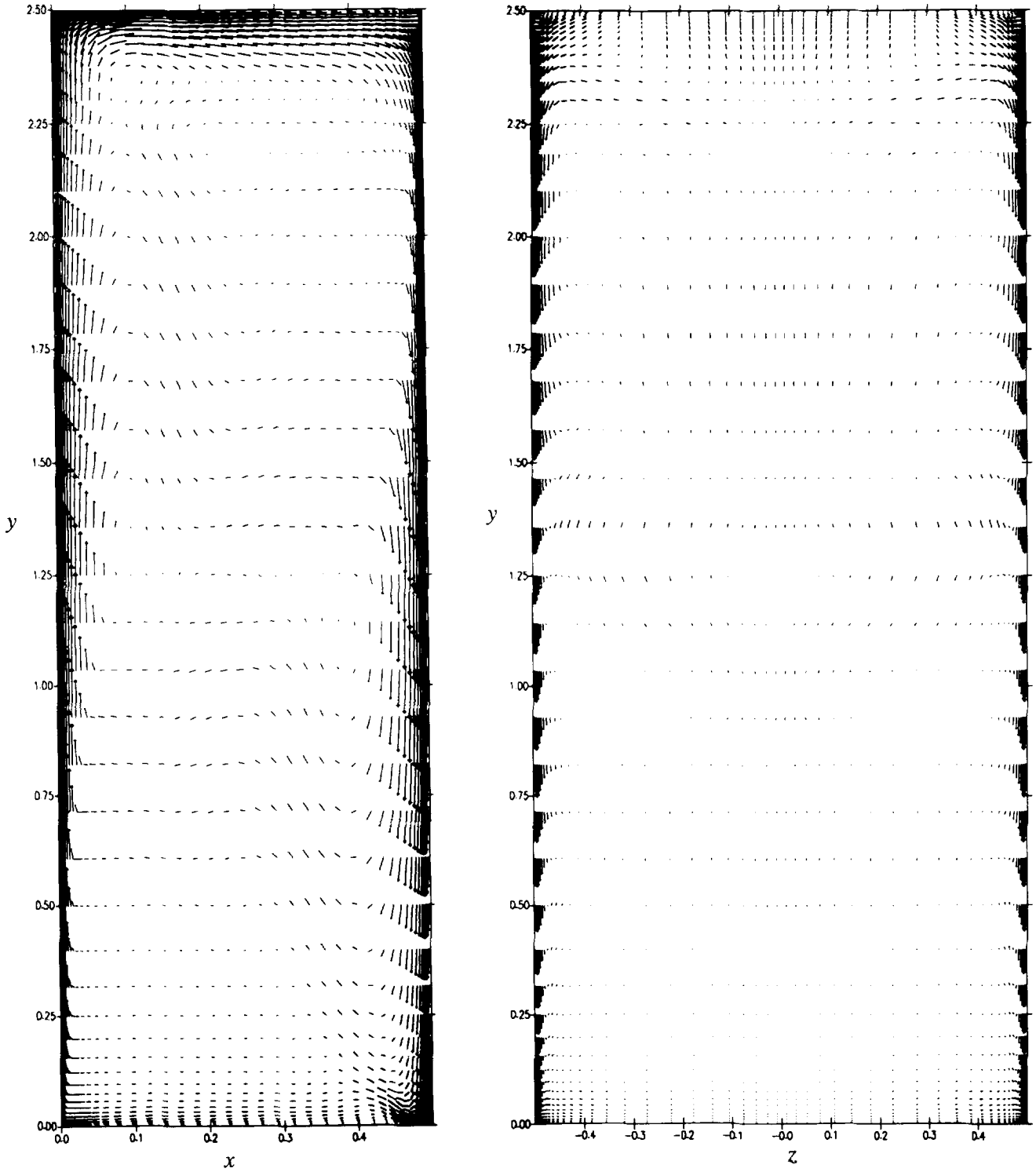

Figure 4 Mean velocity vectors on vertical symmetry planes of cavity; a) primary circulation on x–y plane; and b) secondary circulation on z–y plane

Figure 4a presents the conventional x y plane view. Although the velocity vectors are broadly antisymmetric in appearance. the circulation is certainly more vigorous at the top of the cavity than the bottom principally because of the unstable density stratification that results from heat loss through the upper wall. The large resultant change in effective viscosity is evident in Figure 5. Indeed, although, with an insulated top wall, the flow reverts to laminar before descending the cold wall. with heat losses included a still significantly turbulent natural convection layer is present. This is what is mainly responsible for the very asymmetric viscosity profile at midheight. In contrast with the differences at the top of the cavity, for $y/H = 0.05$, the two viscosity profiles are almost the same, the flow reverting to laminar because of the stable stratification (marginally *more* stable in the case where heat losses occur). Figure 4b shows the corresponding velocity vectors on the other vertical symmetry plane* plotted to the same scale as those in Figure 4a. We note that there is a significant flow down the "insulated" walls, especially in the upper half of the cavity. A further striking feature is the variations in sign of the velocity in the interior of the cavity: for example, along the midplane $y/H = 0.5$, the flow is downward; whereas, just above it, the secondary motion is of similar magnitude, but is directed upwards.

The effects of these three dimensionalities and heat losses on the Nusselt number are shown in Figure 6. The ordinate shows the vertically averaged Nusselt number divided by the value of this quantity on the symmetry line for the case of zero heat loss through the insulated surfaces. The distribution of this parameter for the case of no heat losses is, in fact, remarkably uniform in the z direction except for z close to 0.5; here the presence of the side wall diminishes the natural convective motion causing a pronounced drop in Nusselt number. The behaviour is similar for the heated wall even when heat losses are permited, except that slightly higher levels of $\overline{Nu}$ occur

* The computations were as noted made only over one vertical half of the duct, results simply being copied to corresponding points on the other side of the symmetry plane.

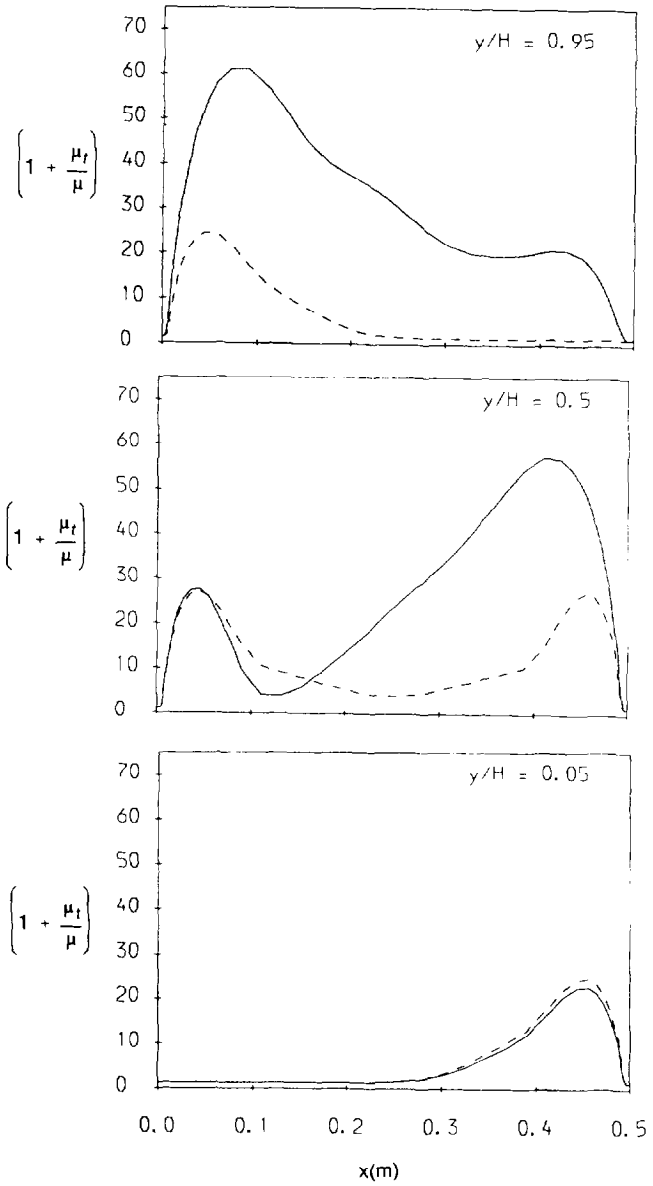

Figure 5 Effective viscosity distribution at $z = 0$; key as in Figure 2

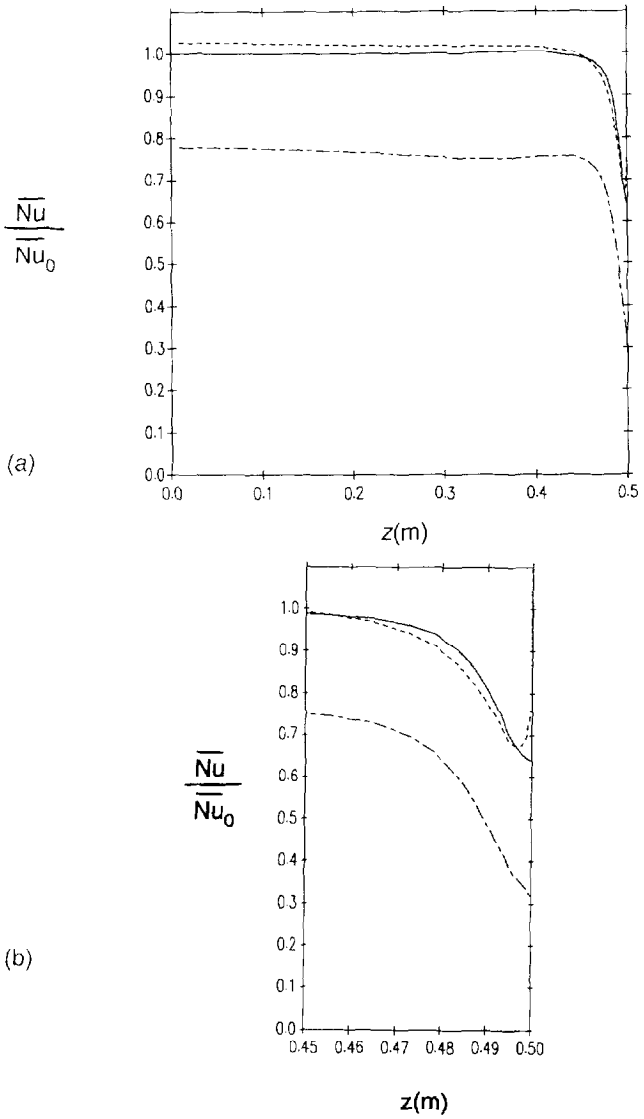

Figure 6 Variation of vertically averaged Nusselt number over active walls; ——— adiabatic secondary surfaces; - - - - - hot wall, with heat losses; and - — - — - cold wall with heat losses; a) complete section from center plane to side wall; and b) detailed behavior near side wall

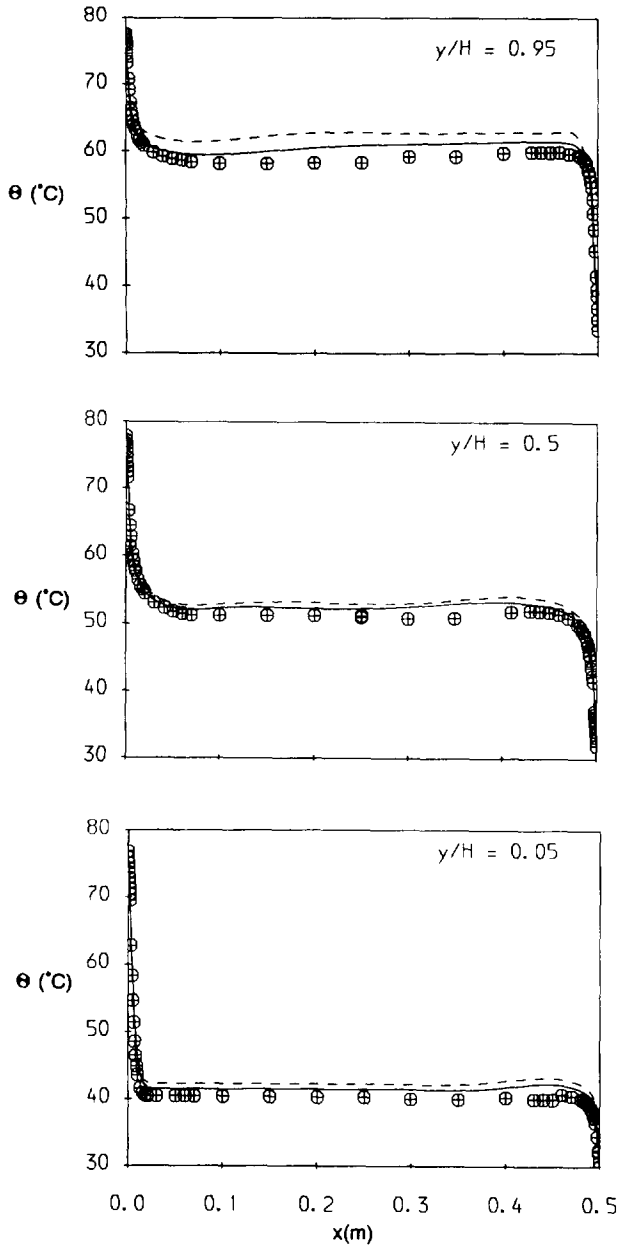

Figure 7 Comparison of 2-D and 3-D computations of temperature on the midplane: ⊕ experiments, Cheesewright et al. (1986); —— 3-D computations with heat losses; and - - - 2-D computations with heat losses

because of the more vigorous velocities that arise in this case. Indeed, there is a significant rise in $\overline{Nu}$ very close to the side wall associated with the appreciable downflow induced by heat leakage through the side wall (see Figure 4). The Nusselt numbers for the cold wall are appreciably lower simply because some 20% of the heat entering the cavity through the heated wall actually leaves through the insulated surfaces.

Although the 3-D results discussed above are the most complete simulation, Figure 7 compares the thermal field on the plane *ABCD* with 2-D computations. The temperature profiles are nearly the same in the lower half of the cavity as found for the 3-D computations, although, near the top of the cavity, the core fluid in the 2-D computation becomes significantly warmer and, thus, further from the experimental behavior. The corresponding differences in the mean velocity profiles, Figure 8, are, however, fairly small. The turbulent viscosity for the 3-D simulation is, nevertheless, some 10% higher, Figure 9, because, apparently, of the additional straining associated with the z-direction gradients.

Conclusions

The study explored the extent to which failures of earlier predictions of the cavity flows of Cheesewright and co-workers (1982; 1986) could be attributed to the fact that these studies did not account for heat losses from nominally adiabatic surfaces or for 3-D effects. It was, indeed, found that accounting for both these factors led to much closer agreement with experiment than hitherto. Although both contributions were significant and acted in the same sense, accounting for heat

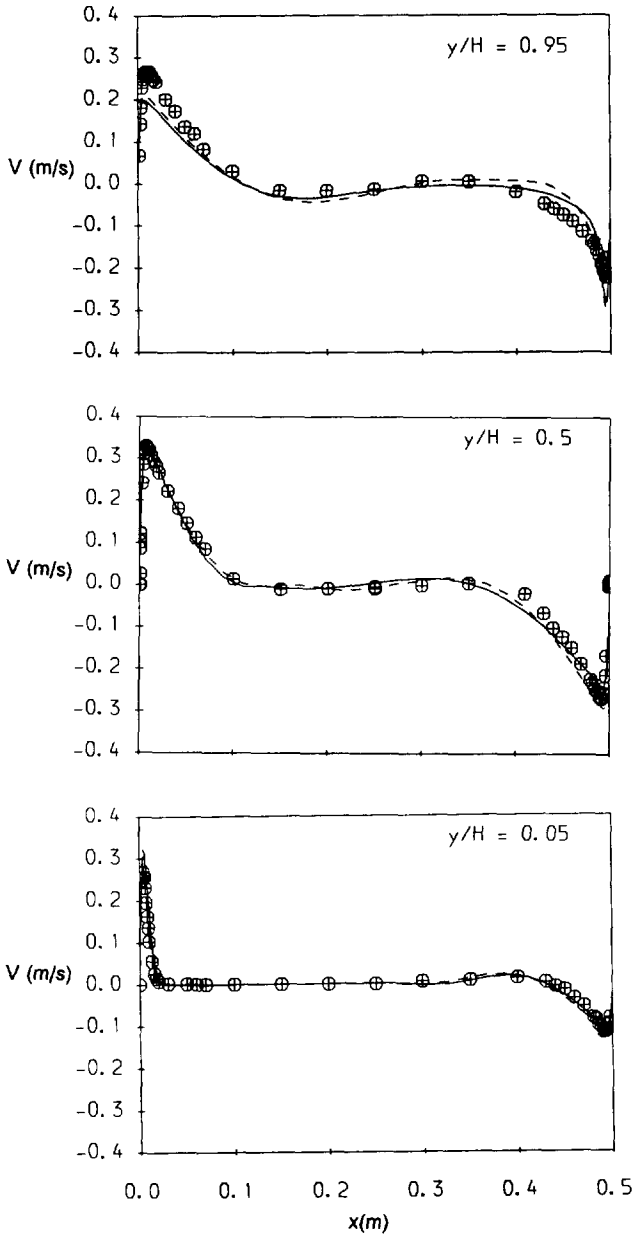

Figure 8 Comparisons of 2-D and 3-D computations of vertical velocity on midplane; key as in Figure 7

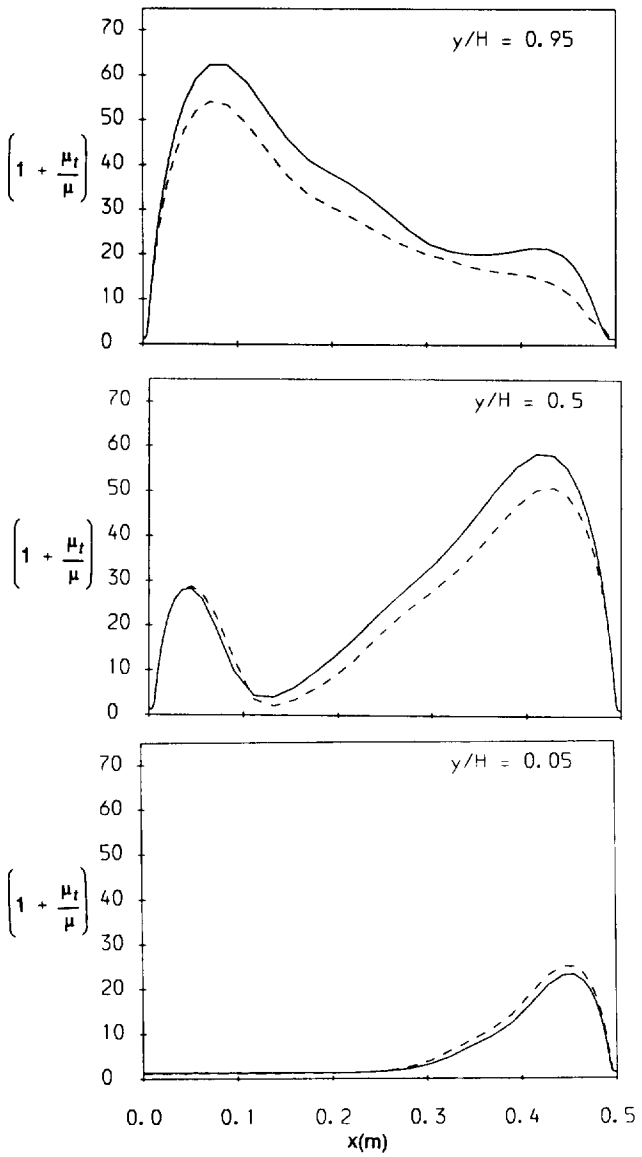

Figure 9 Comparisons of 2-D and 3-D computations of turbulent viscosity on midplane; key as in Figure 7

losses through the top of the cavity could be said to be the most important single contribution.

Acknowledgments

Computational resources provided by the Mechanical Engineering Department of UMIST are gratefully acknowledged. Authors' names are sequenced alphabetically.

References

Cheesewright, R. and Ierokipiotis, F. 1982. *Proc. 7th Int. Heat Transfer Conf.*, **2**, 305–391

Cheesewright, R., King, K. J. and Ziai, S. 1986. Experimental data for the validation of computer codes for the prediction of two-dimensional buoyant cavity flows. In *Significant Questions in Buoyancy-Affected Closure or Cavity Flows*, HTD-60 p75, ASME Winter Annual Meeting

Daly, B. J. and Harlow, F. H. 1970. Transport equations in turbulence. *Phys. Fluids*, **13**, 2634

Huang, P. G. and Leschziner, M. A. 1983. An introduction and guide to the computer code TEAM, UMIST, Mech. Eng. Dept. Rept., University of Manchester, UK

Ince, N. Z. and Launder, B. E. 1989. On the computation of buoyancy-driven turbulent flows in rectangular enclosures. *Int. J. Heat Fluid Flow*, **10**, 110

Ince, N. Z., Betts, P. L. and Launder, B. E. 1993. Low Reynolds number modeling of turbulent cavity flows. In *Turbulent Natural Convection in Enclosures*, R. A. Henkes and C. J. Hoogendoorn (eds.). Editions Européennes Thermique et Industrie, Paris, 76–87

Launder, B. E. 1988. On the computation of convective heat transfer in complex turbulent flows. *J. Heat Trans.*, **110**, 1112–1118

Leonard, B. P. 1979. A stable and accurate convective modeling procedure based on quadratic upstream interpolation. *Comp. Meth. Appl. Mech. Eng.*, **19**, 59

Ozisik, M. N. 1977. *Basic Heat Transfer*, McGraw-Hill, New York